Validation of multicomponent lattice Boltzmann equation simulations using theoretical calculations of immiscible drop shape

I. Halliday, T. J. Spencer,* and C. M. Care
Materials & Engineering Research Institute, Sheffield Hallam University, Howard Street, Sheffield, S1 1WB, United Kingdom
(Received 1 July 2008; revised manuscript received 10 December 2008; published 26 January 2009)

Quantitative comparison between the measured deformation of a neutrally buoyant drop, obtained with an appropriately conceived three-dimensional, multicomponent lattice Boltzmann equation simulation methods for continuum multicomponent hydrodynamics [Phys. Rev. E **76**, 026708 (2007); 76, 026709 (2007)], are shown to be in agreement with the theoretical predictions of Taylor and Acrivos [J. Fluid. Mech. **18**(3), 466 (1964)].

DOI: 10.1103/PhysRevE.79.016706 PACS number(s): 47.11.−j, 47.55.D−, 47.61.Jd

I. INTRODUCTION

The need for careful, validation of the multicomponent lattice Boltzmann (MCLB) equation simulation method [1] must increase as the level of uptake of the method, in, e.g., microfluidics [2] increases. In 2002, Tolke *et al.* compared the measured terminal velocity of drops, obtained with one MCLB variant [3], to analytic results but, to date, we believe that no other quantitative and direct evaluation of MCLB method's interfacial hydrodynamics has been undertaken. Our purpose in this short article is to update matters by performing a challenging and discriminating validation of our most recent MCLB algorithm, using for purposes of quantitative comparison, analytical calculations of suspended drop shapes, due to Taylor and Acrivos [4].

In fact, a match to Taylor and Acrivos' calculation [4] is a demanding test for any of the main MCLB algorithms available [3,5,6] because, to conform with this analysis, it is necessary, among other things, to keep both Reynolds number Re and Weber number Wb small, to observe delicate shape changes which would be corrupted by simulation method artifacts such as interface pinning and faceting [7], and to simulate surprisingly large systems, in order to match Taylor and Acrivos' assumption of rest fluid at infinity.

This article is organized as follows. In Sec. II we setout the background to the calculation we seek to perform, in Sec. III we show how our continuum multicomponent lattice Boltzmann simulations may be applied to this problem and in Sec. IV we present our results. The detail of the lattice Boltmann method we use, the embedded methodological developments and analysis is, contained in the Appendix.

II. BACKGROUND

In 1964, Taylor and Acrivos [4] calculated the shape of a neutrally buoyant drop of red R, liquid moving at a constant speed U, in a second infinite blue B liquid. The latter was assumed to be at rest at infinity. In the notation of Taylor and Acrivos (used throughout) the Weber and Reynolds numbers of this problem are

$$\mathrm{Wb} = \frac{\rho a U^2}{\sigma}, \quad \mathrm{Re} = \frac{aU}{\nu}, \tag{1}$$

in which a is the undeformed radius, σ the interfacial tension, and all other symbols have their usual meaning. We set Taylor and Acrivos' liquids' viscosity and density contrast parameters set to unity immediately:

$$k = \frac{\nu_R}{\nu_B} = 1, \quad \gamma = \frac{\rho_R}{\rho_B} = 1. \tag{2}$$

In this case, Taylor and Acrivos' expression for the steady, axially symmetric drop shape, (parametrized only by the azimuthal coordinate θ and including the effects of inertia, by perturbing about Re=Wb=0, note) is simplified and may be summarized as follows:

$$\frac{R(\theta)}{a} = 1 + \zeta(\theta), \tag{3}$$

where

$$\zeta(\theta) \approx -\lambda \mathrm{We} P_2[\cos(\theta)] - \frac{63}{140}\lambda \frac{\mathrm{We}^2}{\mathrm{Re}} P_3[\cos(\theta)], \tag{4}$$

in which $R(\theta)$ is the radial distance, from the drop center of mass, to the surface element with azimuthal coordinate θ, P_n denotes the Legendre polynomial of degree n, and, for $k=\gamma=1$, we compute that the constant $\lambda = 9/40$. The deformation $\zeta(\theta)$ given in Eq. (4) (the exclusive concern of this article) is measured in the centre of mass frame, so that [4]:

$$\int_{-1}^{+1} \zeta(\theta) d[\cos(\theta)] = 0. \tag{5}$$

For the expression in the right-hand side of Eq. (4) accurately to describe a deformed drop it is clearly necessary to have $\mathrm{Wb}/\mathrm{Re} < 1$, in order to ensure the diminishing importance of higher order terms, which are not calculated. It is also important to note that Taylor and Acrivos' prediction, which is supported by experiment [4,8], assumes at the fluids' interface, a kinematic condition of mutual impenetrability holds, the no traction stress condition and that the difference between the fluids normal interfacial stress contraction

*t.j.spencer@shu.ac.uk

is balanced by interfacial tension [9]. Accordingly, it represents a stringent test of the representation of appropriate boundary conditions within our MCLB.

III. METHOD

We use an MCLB model for three-dimensional axisymmetric flow, which is based on the rectangular D2Q9 single component, single relaxation time variant [1] of Qian *et al.* [10], detailed in Refs. [11,12], but generalized by the addition of a geometrical source term, which modifies the plane Cartesian x-y Navier-Stokes and continuity equations, with additional terms to produce an axially symmetric r-z description. That is, the y (x) Navier-Stokes equation may be transformed into its cylindrically symmetric radial (axial) counterparts. In the Appendix we develop and analyze an appropriate multicomponent lattice Boltzmann method. Based as it is on the work reported in Refs. [11,12], the interface model outlined in this Appendix is designed to produce passive advection of the component-distinguishing phase field function ρ^N and hence our MCLB model's interface, and it has an effective kinematic condition, to optimize correspondence to continuum regime multicomponent hydrodynamics.

Simulations of initially spherical drops, placed on large rectangular lattices, closed with periodic boundaries left to right, to facilitate drop motion and second-order accurate no-slip [13] conditions top to bottom, to inject dissipation, were calibrated by mapping the Reynolds and Weber numbers as follows (an asterisk indicates the corresponding lattice quantity):

$$\mathrm{Re} = \frac{aU}{\nu} \rightarrow \frac{a^* \Delta x U^* \dfrac{\Delta x}{\delta_t}}{\dfrac{1}{6}(2\tau - 1)\dfrac{\Delta x^2}{\delta_t}} = \frac{6a^* U^*}{2\tau - 1} = \mathrm{Re}^*, \tag{6}$$

$$\mathrm{Wb} = \frac{\rho a U^2}{\sigma} \rightarrow \frac{\rho a^* \Delta x U^{*2} \dfrac{\Delta x^2}{\delta_t^2}}{c_s^2 \Delta\rho \dfrac{\Delta x^2}{\delta_t^2} a^* \Delta x} = \frac{\rho U^{*2}}{c_s^2 \Delta\rho^*} = \mathrm{Wb}^*, \tag{7}$$

where τ is the LBGK relaxation time parameter, Δx (δ_t) are its spatial (time) steps, c_s is the speed of sound, and $\Delta\rho$ the interfacial density step. Note that in establishing the above mappings we have used the usual expressions for the lattice fluid viscosity and fluid pressure [1] and, also, the Laplace Law. After a period of equilibration, the red drop fluid was subject to a small, uniform body force to produce uniform motion relative to red background.

Significantly, to first order, the error in measured Wb*:

$$\delta(\mathrm{Wb}^*) = \frac{1}{c_s^2}\left(\frac{\delta a^*}{a^*} + \frac{\delta U^*}{U^*} + \frac{\delta(\Delta\rho)}{\Delta\rho}\right) \tag{8}$$

is relatively large, because the small interfacial tensions required, to promote measurable deformation and to restrict the magnitude of the spurious velocities, only produce a small interfacial density step, $\Delta\rho$. Note also that the calculations of Taylor and Acrivos [4] apply to a system at rest at infinity and that essential dissipation can only be inserted into the corresponding simulations by imposing an explicit rest boundary, which precludes the exclusive use of periodic boundary conditions and force the system to be of finite size.

To make discriminating comparison with the calculations of Taylor and Acrivos it is necessary to avoid the large error associated with a measurement of We*. Accordingly, we choose to measure amplitudes $\langle P_2|\zeta\rangle$ and $\langle P_3|\zeta\rangle$, as detailed shortly, and to assess a relationship between them. This relationship is very simply extracted by using Eq. (4) and a little algebra, which reveals

$$\frac{\langle P_2|\zeta\rangle\langle\zeta|P_2\rangle}{\langle P_3|\zeta\rangle} = \frac{1}{2}\mathrm{Re}^*. \tag{9}$$

Amplitudes $\langle P_1|\zeta\rangle \cdots \langle P_4|\zeta\rangle$ were evaluated by means of a conjugate gradients grid search optimization of the coefficients $a_1 \cdots a_4$ in the finite expansion

$$\zeta(\theta_i) = a_2 P_2(\theta_i) + a_3 P_3(\theta_i) + a_4 P_4(\theta_i), \tag{10}$$

where θ_i is the discrete azimuthal coordinate of a point on the interface (see below). As as consequence of the orthogonality of Legendre polynomials, $a_j = \langle P_j|\zeta\rangle$. Note that the expression in the right-hand side of Eq. (10) includes the uncalculated contribution from P_4, to which point we shall return.

A few remarks are in order before proceeding. (i) In the expansion in Eq. (10), the coefficient a_1 describes the centre of mass translation, (ii) for simulation data which conforms to the assumptions implicit in the calculations of Ref. [4], the following inequalities must hold:

$$|a_2| > |a_3| > |a_4|, \quad \mathrm{Re} \ll 1, \quad \mathrm{Wb} \ll 1, \quad \frac{\mathrm{Wb}}{\mathrm{Re}} \ll 1, \tag{11}$$

and (iii) Taylor and Acrivos do not compute and expression for a_1 and a_4.

In Refs. [11,12] the interface between completely immiscible red and blue fluids is identified by contours of constant value in phase field function

$$\rho^N = \frac{\rho_R - \rho_B}{\rho_R + \rho_B}, \tag{12}$$

the (sublattice) contour $\rho^N = 0$ defining the centre of the interfacial region. Both our target calculations and simulation have explicit cylindrical symmetry, accordingly, measured interfacial position coordinates refer to the centre plane of the drop. Sublattice positions x on the contour $\rho^N = 0$ were determined in by second-order interpolation on the x coordinate, of the phase field defined in Eq. (12). At steady state, the drop centre of gravity having been measured, we computed the angular coordinate θ_i of points on the interface, the corresponding radial distance from the centre of mass r_i, and the deformation

$$\theta_i = \tan^{-1}\left(\frac{y^*}{x}\right), \quad r_i = \sqrt{x^2 + y^{*2}}, \quad \zeta(\theta_i) = \frac{r_i}{a} - 1. \tag{13}$$

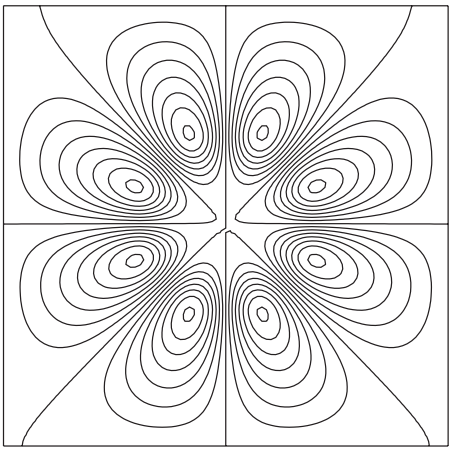

FIG. 1. Rectangular stream function of the spurious flow (or interfacial microcurrent) of a centrally placed circular drop, initial radius 20 lattice units, on a lattice of 100×100 lattice units. Data were obtained for separated fluids with relaxation parameters $\omega_R=\omega_B=1.0$. The maximum spurious velocity occurs where stream function contours are densest, which corresponds to the center of the interfacial region.

Considerable care was found to be necessary to ensure that simulations conformed with the conditions of the target calculations [Eq. (11) above]. Most surprising were the size of the external flow domain necessary to ensure the inequality

$$\langle P_2|\zeta\rangle > \langle P_3|\zeta\rangle \gg \langle P_4|\zeta\rangle, \tag{14}$$

and the simulation times to reach the steady state.

IV. RESULTS AND DISCUSSION

For all data presented, the lattice interfacial tension parameter was $\sigma^*=1.0\times10^{-4}$ [11], the initial red drop radius was 20 lattice units. Drop terminal velocities were typically $o(10^{-4})$ lattice units per time step. Appropriate Re and Wb were calculated from Eqs. (6) and (7). Fluids' collision parameters were the ranges $1.0<\omega_{R/B}<1.4$. For the valid deformation data presented below, it became apparent that the system dimensions, expressed in terms of the initial drop radius a^* were required to exceed a length of approximately $40a^*$ between periodic images and (i.e., in the flow direction) and a transverse distance of approximately $2a^*$ from the symmetry axis to the cylindrical, no-slip boundary.

Clearly, care must be exercised to restrict error associated with spurious velocities, induced by the interface algorithm [11]. Figure 1 is a rectangular stream function, evaluated in the center plane of the simulation, associated with spurious flow. The spurious velocity has a maximum value in the central interface. Figure 2 shows that the variation of the maximum measured value of the spurious velocity $v_{\max}$ in lattice units, divided by the product of the collision parameters, varies weakly with collision parameters, as was first noted by Gunstensen *et al.* [14]. Gunstensen *et al.* also pointed out that microcurrent activity should be, broadly, proportional to the interfacial tension parameter (constant for this data set, note). For present purposes, we remark that, for all data presented here, the spurious flow has entirely negligible effects

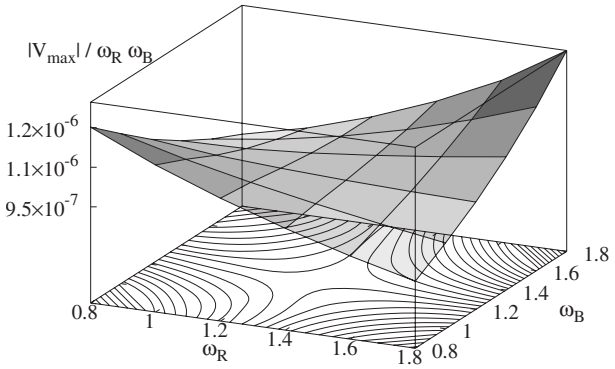

FIG. 2. Maximum microcurrent velocity $v_{\max}$ divided by the product of the collision parameters for the range of the latter used in measurements of deformation. All data were obtained with interfacial tension parameter $\sigma^*=1.0\times10^{-4}$, used for all the data presented.

$$\frac{v_{\max}}{U^*} < \frac{1.26\times10^{-6}}{7.9\times10^{-4}} = 1.53\times10^{-3}, \tag{15}$$

where we have take the value of U^* which characterizes the data of Fig. 3, discussed below.

The dominant contribution, of amplitude $\langle P_2|\zeta\rangle$, corresponds to an oblate deformation, as demonstrated in the data of Fig. 3. The latter shows, as a function of the azimuth θ, the computed oblate deformation of a drop of initial radius 20 lattice units, with a measured steady-state velocity of $U^*=7.9\times10^{-4}$ lattice units per time step and a very small interfacial pressure step of 1.7×10^{-5} lattice units, corresponding to physical Wb=0.074 [Eq. (7)] and physical Re =0.222 [Eq. (6)], Wb/Re=0.33. The simulation lattice dimension was 800×600 lattice units. Measured interfacial

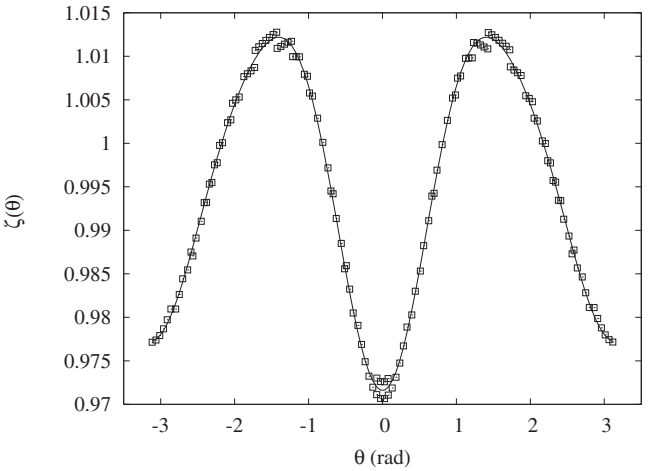

FIG. 3. Measured steady-state deformation of a drop of initial radius 20 lattice units with physical Wb=0.107, Re=0.221. Measured interfacial points are shown as open squares; the solid line corresponds to the optimum fit to Eq. (10), for which the measured amplitudes are given in Table I.

TABLE I. Comparison of measured amplitudes with associated theoretical values. The latter were obtained from Eq. (4) with Wb =0.074, Re=0.222. The data tabulated here corresponds to the data shown in Fig. 3, for which inequalities (11) are valid.

Amplitude	Measured value	Theoretical value	Ratio
$\langle P_2\|\zeta\rangle$	2.33×10^{-2}	1.60×10^{-2}	0.71
$\langle P_3\|\zeta\rangle$	4.53×10^{-3}	2.49×10^{-3}	0.55
$\langle P_4\|\zeta\rangle$	1.72×10^{-3}		

points are shown as open squares; the solid line corresponds to the optimum fit to Eq. (10), obtained as outlined above with computed, amplitudes (grid-searched coefficients a_2–a_4), together with Taylor and Acrivos' theoretical values (evaluated with Wb=0.074, Re=0.222), are summarized in Table I. We note that this data satisfies all the required inequalities, expressed in Eq. (11).

To illustrate the need for care in selecting simulation parameters, and, in particular, the need to calculate the coefficient a_4, Fig. 4 and Table II show equivalent results for Wb=0.021, Re=0.019, this time with ratio Wb/Re=1.09. This data was obtained for a narrower lattice, of 800×400, lattice units. Now, the measured value of the unpredicted coefficient a_4 has the largest value. The convergence of the expression in Eq. (4) is therefore called into question, by the fact that inequalities in Eq. (11) are not all met and there is a qualitative difference between the deformations represented in Figs. 3 and 4.

Returning to the data of Fig. 3 and Table I, it is possible to reassess this data, avoiding the error associated with the Weber number Wb, Eq. (8). We evaluate the left-hand side of Eq. (9) with the data of Table I:

$$\frac{\langle P_2|\zeta\rangle\langle\zeta|P_2\rangle}{\langle P_3|\zeta\rangle} = \frac{(2.33\times10^{-2})^2}{4.53\times10^{-3}} = 0.119, \tag{16}$$

which is within 7% of (half the value of) the measured Reynolds Number for this data. Given the testing nature of this

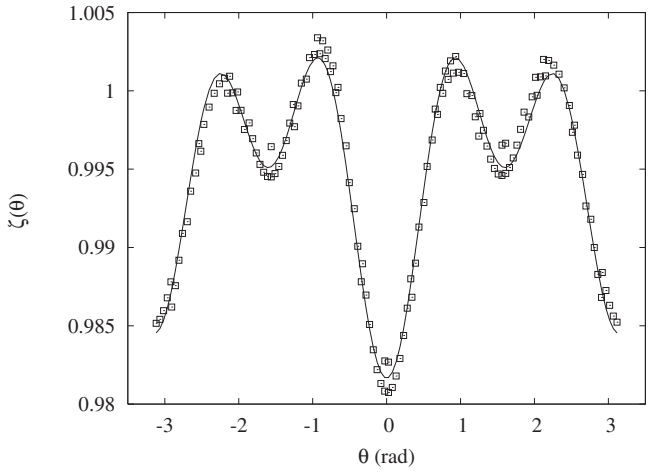

FIG. 4. Measured steady-state deformation of a drop of initial radius 20 lattice units with physical Wb=0.021, Re=0.019. Measured interfacial points are shown as open squares; the solid line corresponds to the optimum fit to Eq. (10), for which the measured amplitudes are given in Table II.

TABLE II. Comparison of measured amplitudes with associated theoretical values. The latter were obtained from Eq. (4) with Wb =0.021, Re=0.019. The data tabulated here corresponds to the data shown in Fig. 3, for which inequalities (11) are not all valid.

Amplitude	Measured value	Theoretical value	Ratio
$\langle P_2\|\zeta\rangle$	3.57×10^{-3}	4.64×10^{-3}	0.77
$\langle P_3\|\zeta\rangle$	1.43×10^{-3}	2.98×10^{-3}	0.64
$\langle P_4\|\zeta\rangle$	5.37×10^{-3}		

validation (the maximum to minimum surface deformation shown in Fig. 3 is about 5% of the undeformed initial drop radius) this agreement is excellent.

For any simulation of sufficient size, conforming with the conditions set out in Eq. (11), the degree of agreement obtained by direct comparison between measured deformation and Taylor and Acrivos' expression is typified by that in Table I.

V. CONCLUSION

A direct, qualitative comparison between the measured deformation of a drop, obtained with a three-dimensional version of our current multicomponent lattice Boltzmann equation simulation method for completely immiscible continuum, multicomponent fluids [11,12] with the analytical predictions of Taylor and Acrivos [4] reveals reasonable quantitative agreement, as shown in Table I. By recasting this data to avoid the error in the measured Weber number [see Eq. (8)] the agreement becomes excellent. These results tend to demonstrate that an appropriate form of multicomponent lattice Boltzmann simulation can be applied with confidence to continuum scale hydrodynamics.

APPENDIX A

In this appendix we present an account of the lattice Boltzmann model used in this article, together with supporting methodological developments and analysis.

1. Continuum multicomponent lattice Boltzmann simulation

Several multicomponent lattice Boltzman (MCLB) algorithms exist, distinguished by the different ways in which fluid-fluid interfaces arise [14–18]. In mesoscale problems, where the kinematics of phase separation feature, Swift's method [15,17], based as it is upon Cahn-Hilliard theory, represents an appropriate choice of MCLB algorithm. For present purposes, the problem we aim to address contains completely immiscible liquid-liquid mixtures, considered in the continuum approximation. For such an application, that MCLB method with appropriate interfacial kinematics and dynamics, developed in Refs. [11,12], is a synthesis of the interface algorithm of Lishchuk *et al.* [18] and the method of Guo *et al.* [19], which correctly encapsulates a spatially variable external force and a component phase field for interfacial tension.

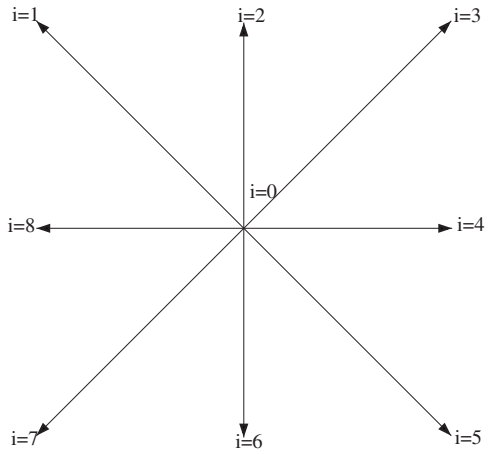

FIG. 5. The relative orientation of the nodal velocity set and subscripting convention for the two-dimensional, nine velocity D2Q9 lattice. Note that, in general, $|\mathbf{c}_{i\text{even}}|=\frac{\Delta x}{\delta_t}$. Note also that links classified with odd values of subscript i have a larger length. The weights corresponding to the links shown here are listed in Table III.

Lishchuk's method recovers continuum level stress boundary conditions applied over an interface between completely separated fluids [9]. The interface is identified by the coupled phase field. Here, our MCLB has a Lishchuk interface maintained by a fluid-fluid segregation step which uses an algorithmically simple and very robust process after one first devised by d'Ortona *et al.* due to Latva-Kokko *et al.* [20] which has been shown to have correct continuum properties [11] and to allow simple modifications which impart a behavior approaching continuum kinematics [12]. The interface methods outlined above may be used with a range of single-component LB variants. Here we use the popular single-component, isothermal, single relaxation-time LBGK model of Qian *et al.* [21], designated D2Q9 [1]. As with all LB, its dynamics is a collision followed by a propagation, over interval δ_t, of a single-particle distribution function f_i forced described by an evolution equation source term $\phi_i(\mathbf{r})$:

$$f_i(\mathbf{r}+\delta_t\mathbf{c}_i,t+\delta_t)=f_i^{\dagger}(\mathbf{r},t)$$
$$=f_i(\mathbf{r},t)-\omega\delta_t[f_i(\mathbf{r},t)-f_i^{(0)}(\rho,\rho\mathbf{u})]+\phi_i(\mathbf{r}). \tag{A1}$$

In Eq. (A1), the right- (left-) hand side represents collisions (propagations). $f_i^{\dagger}(\mathbf{r},t)$ denotes a post-collision value of distribution function. Source term ϕ_i carries the effect of a macroscopic body force density $\mathbf{F}(\mathbf{r},t)$ (which may be the sum of different contributions) on the lattice fluid, as discussed below. Discrete velocity vectors (or links) $\mathbf{c}_i$ form the lattice basis. We use the D2Q9 lattice depicted and indexed in Fig. 5. Each velocity, or link, has an associated weight t_p defined in Table III. Parameter $\omega:0\leqslant\omega\leqslant2$ controls the kinematic viscosity of the fluid $\nu=\frac{1}{6}(\frac{2}{\omega}-1)\frac{\Delta x^2}{\delta_t}$, where Δx is the lattice spacing. In Eq. (A1), ρ is the macroscopic fluid density and $\mathbf{u}$ its velocity: these quantities determine the equilibrium component of the distribution function $f_i^{(0)}(\rho,\rho\mathbf{u})$, which is defined by Guo *et al.* [19], in their Eq. (3). From distribution function f_i [or, indeed, $f_i^{(0)}(\rho,\rho\mathbf{u})$] there emerge macroscopic observables

TABLE III. The link weights t_p and indexing for the D2Q9 lattice depicted in Fig. 5.

i	0	even	odd
$\lvert\mathbf{c}_i\rvert$	0	1	$\sqrt{2}$
t_p	4/9	1/9	1/36

$$\rho=\sum_i f_i, \tag{A2}$$

$$\rho\mathbf{u}=\frac{1}{\rho}\sum_i f_i\mathbf{c}_i+\frac{\delta_t}{2}\mathbf{F}, \tag{A3}$$

which satisfy the usual Cartesian continuity equation and a weakly compressible form of the Navier-Stokes equation, with a $o(1)$ sonic speed and an external body force

$$\frac{\partial}{\partial t}\rho+\frac{\partial}{\partial x_\beta}\rho u_\beta=0, \tag{A4}$$

$$\frac{\partial}{\partial t}\rho u_\alpha+\frac{\partial}{\partial x_\beta}\rho u_\beta u_\alpha=\frac{1}{3}\frac{\partial}{\partial x_\alpha}\rho+\frac{\partial}{\partial x_\beta}(2\rho\nu(\omega)S_{\alpha\beta})+F_\alpha, \tag{A5}$$

where $\nu(\omega)$ is given above. Here $S_{\alpha\beta}$ is the strain rate tensor and the model's sonic speed (the coefficient of the density variation) $c_s^2=\frac{1}{3}\frac{\Delta x^2}{\delta_t^2}$, for our particular D2Q9 base model [1].

As we shall see, separate contributions to the macroscopic external force, F_α, are necessary for interfacial effects (ie. Laplace pressure and no-traction stress conditions) and to allow for the presence, given cylindrical symmetry, of geometrical source terms. Note that in this appendix the summation convention applies only to repeated Greek subscripts.

Using Chapman-Enskog expansion [1,22] on equation (A1), Guo *et al.* determine the evolution equation source term in equation (A1), $\phi(\mathbf{r})$, in terms of the macroscopic external force, $\mathbf{F}(\mathbf{r})$:

$$\phi_i(\mathbf{r})\equiv t_p\left(1-\frac{\omega}{2}\right)(3(\mathbf{c}_i-\mathbf{u})+9(\mathbf{c}_i\cdot\mathbf{u})\mathbf{c}_i)\cdot\mathbf{F}(\mathbf{r}), \tag{A6}$$

which expression accords, to $o(u)$, with that derived much earlier by He, Chen and Doolen [23], from an *ab initio* second-order accurate integration of the forced Bhatnagar-Gross-Krook equation [24].

2. Methodological developments

It is very important to note that Eq. (A6) incorporates the effects of a variable body force into the Navier-Stokes equations (A5) but it leaves the form of the continuity equation unadjusted.

In order to insert into the Cartesian Navier-Stokes and continuity equations so-called geometrical source terms, we

require a spatially variable scalar source term in the continuity equation, denoted $A(\mathbf{r})$:

$$\partial_t \rho + \partial_\alpha v_\alpha = A. \tag{A7}$$

The appropriate form of A will be specified below.

We note that Halliday *et al.* [25] and later Reiss *et al.* [26] have previously developed lattice Boltzmann method schemes for geometrical source terms. The method of Reiss is particularly effective and consistent: unfortunately both these previous schemes are complicated to apply to multicomponent applications and we proceed with a modification of Guo's methods.

Appropriately to generalize the approach of Guo *et al.* we follow the analysis in Ref. [19] as follows. Using their notation, we follow Guo *et al.* [19] but, here, we take $A \neq 0$: that is, we allow for the presence of the continuity equation source term A. Guo's equation (12) for the flux tensor $\Pi^{(1)}_{\alpha\beta}$ [1] may be shown, by direct but tedious algebra, to acquire an additional term in A:

$$\Pi^{(1)}_{\alpha\beta} = -\frac{\delta_t}{\omega}\left[v_\alpha F_\beta + v_\beta F_\alpha + c_S^2(\partial_\alpha v_\beta + \partial_\beta v_\alpha) - \frac{1}{2}(C_{\alpha\beta} + C_{\beta\alpha}) - A v_\alpha v_\beta \right]. \tag{A8}$$

The above expression for $\Pi^{(1)}_{\alpha\beta}$ may then be used, still following the analysis of Guo *et al.* [19], with a modified choice of their tensor parameter:

$$C_{\alpha\beta} = \left(1 - \frac{\omega}{2}\right)[v_\alpha F_\beta + v_\beta F_\alpha - A v_\alpha b_\beta] - \frac{\omega}{2} c_s^2 A \delta_{\alpha\beta} \tag{A9}$$

so that, from Gou's Eq. (6), we may obtain an expression for an appropriate evolution equation source term ϕ_i, which now depends on the geometrical source A supposed to occur in the continuity equation

$$\phi_i = t_p\left(1 - \frac{\omega}{2}\right)\left[A\Gamma_i + \frac{1}{c_s^2}\mathbf{F}(\mathbf{c}_i - \mathbf{v}) + \frac{1}{c_s^2}(\mathbf{F}\cdot\mathbf{c}_i)(\mathbf{v}\cdot\mathbf{c}_i)\right], \tag{A10}$$

where

$$\Gamma_i = \frac{2 - \omega\left(\dfrac{\mathbf{c}_i\cdot\mathbf{c}_i - 2c_s^2}{2c_s^2}\right)}{2-\omega}. \tag{A11}$$

Eq. (A10) replaces Eq. (A6) for situations in which a continuity equation source term A is required.

As previously stated, for the present situation, the variable body force density $\mathbf{F}$ derived from two independent superposable contributions, one applicable throughout the simulation domain, responsible for geometrical effects (identified below), the other, applicable only in interfacial regions, for interfacial effects. We write

$$\mathbf{F} = \mathbf{F}^i + \mathbf{F}^g \tag{A12}$$

and proceed first to account for contribution $\mathbf{F}^i$ and related segregation effects. Fluid-fluid interface dynamics are applied in regions of the lattice where two immiscible fluids interact (and segregate). The two fluids concerned are designated red and blue. The distribution function f_i is specified for these red and blue fluids individually:

$$f_i(\mathbf{r},t) = R_i(\mathbf{r},t) + B_i(\mathbf{r},t), \tag{A13}$$

with the nodal density of red and blue fluids

$$R = \sum_i R_i, \quad B = \sum_i B_i \tag{A14}$$

conserved. Where fluids mix, the sum fluid evolves according to evolution equation (A1), interface dynamics being captured by the force $\mathbf{F}^i$. The mixture is segregated, by a process which influences the emergent fluids' dynamics, using a phase field $\rho^N(\mathbf{r})$:

$$\rho^N(\mathbf{r},t) \equiv \left(\frac{R(\mathbf{r},t) - B(\mathbf{r},t)}{R(\mathbf{r},t) + B(\mathbf{r},t)}\right), \quad -1 \leqslant \rho^N(\mathbf{r}) \leqslant 1. \tag{A15}$$

Red and blue fluids mix under the propagation step, defining the interfacial region where an external force is applied to the sum fluid, capturing the interfacial effects [18]. In segregation values of R_i and B_i are re-assigned after Latva-Kokko *et al.* [20] and d'Ortona *et al.* [27] using

$$R_i^{\dagger\dagger} = \frac{R}{R+B} f_i^{\dagger} + \beta \frac{RB}{R+B} t_p \hat{f}\cdot\mathbf{c}_i,$$

$$B_i^{\dagger\dagger} = \frac{B}{R+B} f_i^{\dagger} - \beta \frac{RB}{R+B} t_p \hat{f}\cdot\mathbf{c}_i. \tag{A16}$$

in which, e.g., $R_i^{\dagger\dagger}$ denotes a post-collision, post-segregation quantity, $\beta = 0.7$ is an interface thickness parameter, and

$$\hat{f} = -\hat{n} = \frac{\nabla\rho^N}{|\nabla\rho^N|} \tag{A17}$$

is the negative of the local interfacial normal. Use of Eq. (A16), has been demonstrated to produce the following dynamics in the macroscopic phase field [11,12]:

$$\frac{d}{dt}\rho^N = \frac{1}{2\rho}\nabla\left(c_s^2\rho^N\nabla\rho - \rho^N\mathbf{F}\right). \tag{A18}$$

In the interfacial region the principal contribution to the lattice density gradient (the interfacial Laplace pressure step) is the macroscopic surface-tension inducing force, to a good approximation $c_s^2\nabla\rho \approx \mathbf{F}$, and Eq. (A18) closely approximates a continuum kinematic condition of impenetrability $\frac{d\rho^N}{dt} = 0$. We note in passing that variation of the phase field with distance r, measured along a line passing through the local centre of interfacial curvature, is well approximated in two dimensions by

$$\rho^N = \tanh[\beta(r - R)], \tag{A19}$$

where R is local radius of curvature. This fact may be exploited to control changes of viscosity across the interface. To produce a kinematic viscosity variation between red and blue components set:

$$\omega(\rho^N) = \frac{\omega_B(1-\rho^N)}{2} + \frac{\omega_R(1+\rho^N)}{2}, \tag{A20}$$

with ω_R and ω_B again being chosen so that the kinematic viscosity of the red and blue fluids is identical. After Lishchuk *et al.* [18], the Laplace pressure inducing interface force $\mathbf{F}^i(\mathbf{r})$ is proportional to the K local curvature in the ρ^N field

$$\mathbf{F}^i(\mathbf{r}) = \frac{1}{2}\alpha K \nabla \rho^N, \tag{A21}$$

with α the interfacial tension.

In the present work, the system has cylindrical symmetry in which the $\hat{e}_z$ corresponds to $\hat{e}_\phi$ locally. Local curvature, K, was obtained from a surface gradient measured in a local Cartesian system:

$$K = n_x n_y \left(\frac{\partial}{\partial y} n_x + \frac{\partial}{\partial x} n_y \right) - n_x^2 \frac{\partial}{\partial y} n_y - n_y^2 \frac{\partial}{\partial x} n_x, \tag{A22}$$

where, because the interface normal $\hat{n}$ is confined to the plane of lattice n_z and, indeed, all z derivatives have been omitted. In passing we note that all gradients are calculated numerically, from suitable isotropic, finite differences [28] which are accurate to $o(4)$ in Δx, and we emphasize again that the cumulative effect of the force in Eq. (A21) is to produce a Laplace pressure step in a manner consistent with other interface effects, e.g., the no-traction stress conditions [18]. Clearly, for a distributed interface, variation in the measured curvature must occur along the normal direction, which calls into question the accuracy of the process by which the Laplace pressure is imposed. In the next subsection we will demonstrate that any error associated with this effect is small.

We now proceed to consider the second contribution to the macroscopic force acing on the fluid $\mathbf{F}^s$ and the associated continuity equation source. This effective force and continuity source is responsible for introducing the effects of cylindrical symmetry. As such, as is to be applied throughout the simulation domain, not just in interfacial regions. Always constraining the drop centre to lie on the cylindrical system axis $r=0$, and using the mappings

$$(x,y) \to (z,r), \tag{A23}$$

$$(v_x,v_y) \to (V_z,v_r), \tag{A24}$$

the geometrical source terms for the cylindrical polar coordinate form of the continuity equations is

$$A = -\frac{1}{y}\rho v_y, \tag{A25}$$

and the geometrical source terms for the cylindrical polar coordinate form of the Navier-Stokes equation are

$$F_x^g = \frac{\nu}{y}\frac{\partial}{\partial y}\rho v_x, \tag{A26}$$

$$F_y^g = \frac{\nu}{y}\frac{\partial}{\partial y}\rho v_y - \frac{\nu\rho}{y^2} v_y, \tag{A27}$$

which, together with the other force contribution in Eq. (A21) may be incorporated into the expression for $\mathbf{F}$ in Eq. (A12).

With the macroscopic force evaluated, the expression for continuity equation source, given in Eq. (A25), may be used to evaluate evolution equation source term ϕ_i using Eq. (A10). Note that isotropic $o(4)$ accurate finite differences [28] are used to evaluate the gradients in Eqs. (A25)–(A27).

3. Model analysis

In this subsection we set out to demonstrate that the error associated with variation of curvature in Lishchuk's method [18] is, in the context of the present work, entirely negligible. We work in lattice units, in two dimensions, placing the local coordinate origin at the center of the interface, with its x axis lying along the local interface normal. Accordingly, the interface lies confined to region $-\Delta \leqslant x \leqslant \Delta$, where the interface thickness Δ is controlled by parameter β in Eq. (A16). The Laplace pressure step accumulated by the action of force $\mathbf{F}^s$ may be obtained from Eq. (A21) as follows:

$$\Delta P = \frac{\alpha}{2}\int_{-\Delta}^{\Delta} K \frac{d\rho^N}{dx} dx = \frac{\alpha}{2R}\int_{-\Delta}^{\Delta} \left(1 + \frac{x}{R}\right)^{-1} \frac{d\rho^N}{dx} dx, \tag{A28}$$

whence, on using a binomial expansion:

$$\Delta P = \frac{\alpha}{2R}\left[\int_{-\Delta}^{\Delta} d\rho^N + \sum_{n=1} \frac{(-1)^n}{R^n} \int_{-\Delta}^{\Delta} x^n \frac{d\rho^N}{dx} dx \right]. \tag{A29}$$

Now, for symmetric interval $-\Delta \leqslant x \leqslant \Delta$, function $\frac{d\rho^N}{dx}$ has even parity [see Eq. (A19)] so

$$\int_{-\Delta}^{\Delta} x^{2n+1} \frac{d\rho^N}{dx} dx = 0 \tag{A30}$$

and

$$\int_{-\Delta}^{\Delta} d\rho^N = [\rho^N]_{-\Delta}^{\Delta} = 2, \tag{A31}$$

so Eq. (A29) may be simplified to

$$\Delta P = \frac{\alpha}{2R}\left[2 + \frac{1}{R^2}\Gamma_2(\beta\Delta) + \frac{1}{R^4}\Gamma_4(\beta\Delta) + o(R^{-6}) \right], \tag{A32}$$

where we have defined

$$\Gamma_{2n}(\beta\Delta) \equiv \int_{-\Delta}^{\Delta} x^{2n} \frac{d\rho^N}{dx} dx. \tag{A33}$$

Shortly we will drop $o(R^{-5})$ terms from Eq. (A32). Using integration by parts, Eq. (A19) and the substitution $y=\beta x$, definition (A33) becomes

$$\Gamma_{2n}(\beta\Delta) = 2\Delta^{2n}\left(1 - \frac{n}{(\beta\Delta)^{2n}}\int_0^{\beta\Delta} y^{2n-1}\tanh(y)\right)dy. \tag{A34}$$

Now, the practical cutoff for interface force application in simulations is taken to be $|\rho^N| < 0.9995$. Then Δ is implicitly defined through the relation $\tanh(\beta\Delta)=0.999$, hence $\beta\Delta \simeq 5.0$ and, since $\beta=0.7$ in our simulations, it follows $\Delta = 5/0.7 = 7.14$. Accordingly, we estimate the integral in the right-hand side of Eq. (A34) as $\int_0^5 y^{2n-1}\tanh(y)dy$, whereupon, on neglect of terms of $o(R^{-4})$, we are able to evaluate the leading terms in Eq. (A32):

$$\Delta P \approx \frac{\alpha}{R}\left[1 + \frac{7.14^2}{R^2}\left(1 - \frac{2}{5^2}\int_0^5 y\tanh(y)dy\right)\right]. \tag{A35}$$

Clearly the term in round brackets in the right hand of Eq. (A35) represents the principal departure from Laplace law behavior. Using a simple trapezium rule numerical integration, it evaluates to 0.023. For the case of a local radius of curvature $R=20$, this means an error of less that 0.3%. Clearly, error will increase in inverse proportion to (the square of) the local radius of curvature but even for a local radius of curvature as small as $R=5$, it is less than 2.3%.

[1] S. Succi, *The Lattice Boltzmann Equation for Fluid Mechanics and Beyond* (Clarendon Press, Oxford, 2001).
[2] M. M. Dupin, I. Halliday, and C. M. Care, Phys. Rev. E **73**, 055701(R) (2006).
[3] J. Tolke, M. Krafczyk, M. Shulz, and E. Rank, Philos. Trans. R. Soc. London, Ser. A **360**, 535 (2002).
[4] T. D. Taylor and A. Acrivos, J. Fluid Mech. **18**(3), 466 (1964).
[5] M. R. Swift, E. Orlandini, W. R. Osborn, and J. M. Yeomans, Phys. Rev. E **54**, 5041 (1996).
[6] X. W. Shan and H. D. Chen, Phys. Rev. E **49**, 2941 (1994).
[7] I. Halliday, R. Law, C. M. Care, and A. P. Hollis, Phys. Rev. E **73**, 056708 (2006).
[8] W. L. Haberman and R. K. Morton (unpublished).
[9] L. D. Landau and E. M. Lifshitz, *Fluid Mechanics*, Vol. 6, 1st ed. (Pergamon, Oxford, 1959).
[10] Y. H. Qian, D. d'Humières, and P. Lallemand, Europhys. Lett. **17**, 479 (1992).
[11] I. Halliday, A. P. Hollis, and C. M. Care, Phys. Rev. E **76**, 026708 (2007).
[12] A. P. Hollis, I. Halliday, and R. Law, Phys. Rev. E **76**, 026709 (2007).
[13] A. P. Hollis and I. Halliday, J. Comput. Phys. **227**, 8065 (2008).
[14] A. K. Gunstensen, D. H. Rothman, S. Zaleski, and G. Zanetti, Phys. Rev. A **43**, 4320 (1991).
[15] M. R. Swift, W. R. Osborn, and J. M. Yeomans, Phys. Rev. Lett. **75**, 830 (1995).
[16] X. W. Shan and H. D. Chen, Phys. Rev. E **49**, 2941 (1994).
[17] M. R. Swift, E. Orlandini, W. R. Osborn, and J. M. Yeomans, Phys. Rev. E **54**, 5041 (1996).
[18] S. V. Lishchuk, C. M. Care, and I. Halliday, Phys. Rev. E **67**, 036701 (2003).
[19] Z. Guo, C. Zheng, and B. Shi, Phys. Rev. E **65**, 046308 (2002).
[20] M. Latva-Kokko and D. H. Rothman, Phys. Rev. E **71**, 056702 (2005).
[21] Y. H. Qian, D. d'Humieres, and P. Lallemand, Europhys. Lett. **17**, 479 (1992).
[22] S. Hou, Q. Zou, S. Chen, G. Doolen, and A. C. Cogley, J. Comput. Phys. **118**, 329 (1995).
[23] X. He, S. Chen, and G. D. Doolen, J. Comput. Phys. **146**, 282 (1998).
[24] P. L. Bhatnagar, E. P. Gross, and M. Krook, Phys. Rev. **94**, 511 (1954).
[25] I. Halliday, L. A. Hammond, C. M. Care, K. Good, and A. Stevens, Phys. Rev. E **64**, 011208 (2001).
[26] T. Reis and T. N. Phillips, Phys. Rev. E **75**, 056703 (2007).
[27] U D'Ortona, D. Salin, M. Cieplak, R. B. Rybka, and J. R. Banavar, Phys. Rev. E **51**, 3718 (1995).
[28] I. Halliday, R. Law, C. M. Care, and A. P. Hollis, Phys. Rev. E **73**, 056708 (2006).